Ionics (2015) 21:2137–2147
DOI 10.1007/s11581-015-1420-4

ORIGINAL PAPER

Hollow structured Sn-Co nanospheres by galvanic replacement reaction as high-performance anode for lithium ion batteries

Anni Jiang[1] · Xin Fan[1] · Jin Zhu[1] · Daqian Ma[1] · Xinhua Xu[1,2]

Received: 4 June 2014 / Revised: 13 March 2015 / Accepted: 13 March 2015 / Published online: 1 April 2015

Abstract Hollow Sn-Co nanospheres have been fabricated by galvanic replacement reaction. In particular, the hollow resultants with different shell thickness and void space can be obtained using sacrificial templates with different sizes. The structural evolution of Sn-Co hollow microspheres and structure changes during charge/discharge process were studied using XRD, SEM, and TEM. As an anodic material, the hollow resultants with thin shell and relatively large void space exhibited a good reversible capacity of 502 mAh g^{-1} at a current density of 100 mA g^{-1} and a coulomb efficiency over 99 % after 100 cycles. The contributions of the hollow structure and the inactive Co element to electrochemical performance were verified by galvanostatic charge/discharge cycling, electrochemical impedance spectroscope, and TEM measurements. A possible mechanism for hollow structure with different shell thickness to alleviate the volume change was proposed.

Keywords Hollow Sn-Co nanospheres · Galvanic replacement reaction · Anode · Lithium ion battery

Introduction

Owing to their advantages of high operation voltage, no memory effect, and high energy density, lithium ion batteries (LIBs) have been commercially used as power sources for extended applications such as portable electronic devices and electric vehicles [1, 2]. With the growing need for higher capacity and safety, numerous efforts have been made to develop novel anode materials as alternatives to graphite. Among various attractive candidates for anodes, metal tin (Sn) has emerged as a kind of promising anode for next-generation LIBs, since it has a theoretical specific capacity of as high as 993 mAh g^{-1} [3, 4]. However, it has been shown to be difficult to utilize pure Sn due to the severe volume variation (about 300 %) between Sn and $Li_{4.4}Sn$ during cycling. The volume change can cause electrode pulverization and electric disconnection, which is responsible for the poor cyclic life of Sn electrodes [5, 6]. The most common problem-solving strategy employed in the literature is to tailor the particle size of electrochemical materials to nanometer-scale [7–10] and to form intermetallic Sn-based compounds [11–14]. Though the electrochemical performance of Sn-based anodes in literature is improved, it is still not sufficient to meet the practical demands, which implies that the implement of Sn-based electrodes may not be achieved by simply introducing Sn-based alloy at nanoscale.

According to recent research studies [15–19], hollow structure has been developed to further circumvent the issue of volume change. Fang et al. [20] synthesized SnO_2-Fe_2O_3 hollow spheres using a solid acid sphere, as the template and the hollow SnO_2-Fe_2O_3 nanospheres showed excellent cycling performance. The enhancement of the battery performance could be attributed to the structural merit of hollow structure [21, 22]. The large surface area of the hollow structure enables better access for Li^+ as a result of the increased electrode-electrolyte contact area. Moreover, the combination of exterior shell and hollow interior significantly shortens Li^+ transport path, thus resulting in improved electrochemical kinetics of the hollow structure. Besides the large surface area and the

✉ Xinhua Xu
xhxutju@gmail.com

[1] School of Materials Science and Engineering, Tianjin University, Tianjin 300072, People's Republic of China

[2] Tianjin Key Laboratory of Composite and Functional Materials, Tianjin 300072, People's Republic of China

reduced Li^+ diffusion length, the interior cavities can enhance the specific capacity by providing extra space for the storage of Li^+ and improve the cycling stability by buffering against the local mechanical strain associated with repeated Li^+ insertion/extraction process [23]. As a result of the significantly mitigated electrode pulverization and polarization, exceptional electrochemical performance is thus highly anticipated for hollow Sn-based alloy anodes.

Recently, significant efforts have been devoted to the fabrication of hollow structure on the basis of template method, since the utilization of pre-grown templates allows rational design of the size and shape of the resultant hollow structure [24–26]. Nevertheless, these hard or soft template-based methods face many challenges, such as the tedious procedures for shell deposition and template removal. In contrast to the polymer and inorganic nonmetal templates, novel approaches based on sacrificial templates hold great promise in synthesizing hollow nanostructure with well-defined interiors. The sacrificial templates act as consumable resultants for shell construction and can be depleted during the hollowing process. This simple preparation process will avoid the additional problems on the product quality and process cost. Especially for the hollow structure with tiny size (<200 nm), these strategies are particularly attractive due to the convenience of growing shells on high-curvature objects [24, 27]. Generally, there are two main mechanisms using sacrificial template method to obtain hollow resultants, i.e., Kirkendall effect [28–30] and galvanic replacement [31–34]. Compared with Kirkendall effect, galvanic replacement does not require additional surface functionalization, and moreover, it provides a remarkably facile and versatile route to fabricate hollow intermetal nanostructure [27, 33]. However, previous reports are almost limited to noble metal materials. Hollow Sn-based bimetallic nanostructure for LIBs is rare. It is worth mentioning that in galvanic replacement reaction, the void space and shell thickness of the hollow resultants can be easily controlled by tuning the size of sacrificial templates, thus providing the opportunity to further optimize the performance of anode materials [35].

Here, the hollow Sn-Co nanospheres are synthesized by using Co nanoparticles as sacrificial templates via galvanic replacement reaction. In particular, hollow Sn-Co nanospheres with different shell thickness were prepared to investigate the influence of shell thickness on electrochemical performance. Based on the electrochemical results, a possible mechanism for hollow structure to relieve the volume change is proposed. Benefiting from the synergetic merits of the hollow nanostructure along with the nonreactive Co element, the resulting hollow Sn-Co nanospheres could dramatically improve the electrochemical performance.

Experimental

Materials and equipments

All chemicals were of analytical grade and used as purchased without further purification. $C_4H_6CoO_4 \cdot 4H_2O$ (>99.5 %), $SnSO_4$ (>99 %), poly(vinylpyrrolidone) (PVP), sodium borohydride ($NaBH_4$, >98 %), and sodium hydroxide (NaOH, >96 %) were obtained from Kewei Chemical Reagent Co. Ltd. of Tianjin University (Tianjin, China).

The morphology and microstructure of the samples were examined by transmission electron microscopy (TEM, JEM100CXII, 5KV) and field emission scanning electron microscopy (FESEM, S-4800) with energy dispersive X-ray spectrometer. X-ray powder diffraction (XRD, Rigaku D/MAX-2500) was used to examine the alloy components.

Electrochemical measurements of the resultant samples were carried out using two-electrode cells (CR2032) in a glove box. The working electrode was prepared by coating the mixture of prepared active materials, acetylene black, and polyvinylidene fluoride (8:1:1 by weight) in *n*-methyl pyrrolidinone onto Cu substrates and dried at 90 °C for 12 h followed with pressing them at 10 MPa. The mass of active materials on the anode was 0.025 g. The counter/reference electrode was the lithium metal, and the electrolyte solution contained 1 M $LiPF_6$ in a mixture of ethylene carbonate and diethyl carbonate (1:1 by volume). Celgard 2400 was used as the separator. The cell assembly was performed in an Ar-filled glovebox filled with moisture and oxygen concentrations below 1.0 ppm. Galvanostatic charge and discharge measurements were carried out at a constant current density of 100 mA g^{-1} in the voltage range of 0.01–2.0 V by a LAND battery tester. Cyclic voltammetry (CV) was performed on a CHI 660B electrochemical workstation at a scan rate of 0.1 mV s^{-1} in the potential window of 0.001–2.0 V. Electrochemical impedance spectroscopy (EIS) was performed with a frequency range of from 1×10^6 to 0.01 Hz.

Synthesis of Co nanoparticles

Co nanoparticles were synthesized by chemical reduction method. A 0.33 g $C_4H_6CoO_4 \cdot 4H_2O$ and 0.1 g PVP were dissolved in 30 mL glycol. Then, the pH of the solution was adjusted to 12 using 2-M NaOH solution. Afterward, 0.33 g $NaBH_4$ as reducing agent was added into the solution with vigorous stirring at 50 °C. Finally, the mixed solution was stirred for 40 min, and the Co nanoparticles were collected and washed with distilled water and ethanol for several times. The products were obtained by vacuum drying at 200 °C for 2 h. The Co nanoparticles with larger diameters were also prepared by reducing the amount of PVP to 0.01 g. The prepared Co nanoparticles were stored in ethanol for further use.

Synthesis of hollow Sn-Co nanospheres

A 0.1 g of as-prepared Co nanoparticles was initially dispersed in 150 mL distilled water and sonicated to obtain a homogeneous suspension. Then, 0.364 g $SnSO_4$ was added to the suspension at 80 °C under argon atmosphere, and the mixed solution was stirred for 10 h. The ratio of Sn^{2+}/Co was 1:1. After cooling to room temperature, the precipitate was centrifuged and washed with distilled water and ethanol for several times. After annealing at 200 °C for 8 h, the hollow Sn-Co nanospheres were obtained (sample 1). Under the same conditions, Co nanoparticles with a larger diameter were used as sacrificial templates to prepare another type of hollow Sn-Co nanospheres (sample 2). For comparison, pure Sn nanoparticles were synthesized with an average diameter of about 63 nm according to our previous literature [36].

Results and discussion

Figure 1 shows the XRD patterns of the two types of hollow Sn-Co nanospheres utilizing different Co nanoparticles as sacrificial templates. As shown in Fig. 1, the peaks at 28.1°, 32.92°, 35.66°, 38.66°, 40.08°, 43.24°, 43.76°, 45.12°, 56.86°, 58.00°, 60.42°, 62.58°, 65.58°, 68.24°, 68.8°, 71.82°, 81.84°, 83.74°, 86.08°, and 86.34° are assigned to $CoSn_2$ (JCPDS no. 25-0256), and peaks at 28.5°, 30.56°, 31.88°, 33.38°, 33.78°, 35.72°, 40.76°, 42.76°, 43.24°, 46.18°, 52.68°, 59.3°, 62.08°, 63.28°, 66.48°, 69.44°, 73.82°, and 75.4° are attributed to $CoSn_3$ (JCPDS no. 48-1813). The peaks are sharp and intensive, and no residues or contaminants are detected, implying the high crystallization and purity of the samples. Although the size of Co templates is different, the component of the two types of hollow

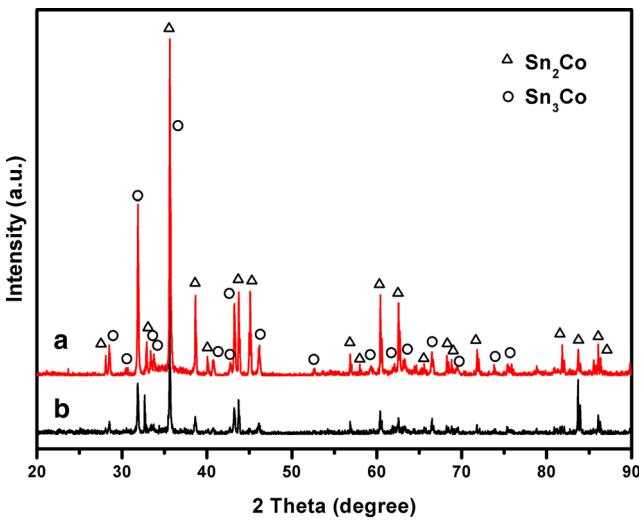

Fig. 1 XRD patterns of as-prepared hollow Sn-Co nanospheres: **a** sample 1 and **b** sample 2

resultants is almost the same. This is attributed to the same galvanic replacement mechanism between bulk Co nanoparticles and Sn^{2+} in the aqueous solution.

Figure 2a, b shows the morphology of the two types of resultant hollow Sn-Co nanospheres, respectively. The inserted SEM images display the morphology of corresponding sacrificial template Co nanoparticles. As shown in Fig. 2a, the solid Co nanoparticles and the corresponding hollow Sn-Co resultants are about 83 and 150 nm in diameter, respectively. It can be also clearly seen in Fig. 2b that the diameter of Co nanoparticles is about 112 nm and that of hollow Sn-Co resultants is about 230 nm. In both cases, the final hollow Sn-Co products possess a uniform spherical shape, closely resembling that of the original template Co nanoparticles. This further confirms that the sacrificial templates directly determine the size and shape of the hollow resultants in galvanic replacement reaction. As shown in Fig. 2a, b, highly uniform hollow structure is obviously visible by the sharp contrast between the Sn-Co shells and the hollow interiors. It should be pointed out that the shell thickness of hollow Sn-Co resultants in two cases is different. The shell thickness of hollow Sn-Co resultants in Fig. 2a is about 20 nm, whereas that in Fig. 2b is about 40 nm. Here, sample 1 and sample 2 are denoted as hollow Sn-Co-20 nanospheres and hollow Sn-Co-40 nanospheres according to the shell thickness of 20 and 40 nm, respectively. Figure 2c, d shows the EDS spectrums of hollow Sn-Co-20 and Sn-Co-40 nanospheres. The weight percentage of Sn in hollow Sn-Co-20 nanospheres is measured to be 83.28 %, and that in hollow Sn-Co-40 nanospheres is 82.54 %. These results reveal that the composition of hollow Sn-Co-20 and Sn-Co-40 nanospheres is almost the same.

Figure 3a shows the high magnification TEM image of hollow Sn-Co-20 nanospheres. From the TEM image, the uniform shell of hollow Sn-Co-20 nanospheres is clearly observed. Meanwhile, Fig. 3b displays the HRTEM image of hollow Sn-Co-20 nanospheres. The lattice spacing of 0.1619 nm corresponds to the (312) plane of $CoSn_2$, and 0.2094 nm relates to the (602) plane of $CoSn_3$, which confirm the nanostructure of hollow Sn-Co-20 nanospheres. To further explore the structural feature, the elemental mapping study of hollow Sn-Co-20 nanospheres is carried out by EDS and presented in Fig. 3c–e. From the mappings, it is found that both Sn and Co compositions exist homogeneously along in the depth direction.

Figure 4 shows the schematic illustration of the major steps at different stages of the galvanic replacement reaction between Co nanoparticles and $SnSO_4$ aqueous solution. In particular, the corresponding TEM images at these four stages are also displayed in Fig. 4a–d to demonstrate morphological and structural evolution in the hollowing process. The driving force for the reaction comes from the difference in reduction potential of the two metals involved. When the $SnSO_4$ solution is added into the Co nanoparticles aqueous suspension,

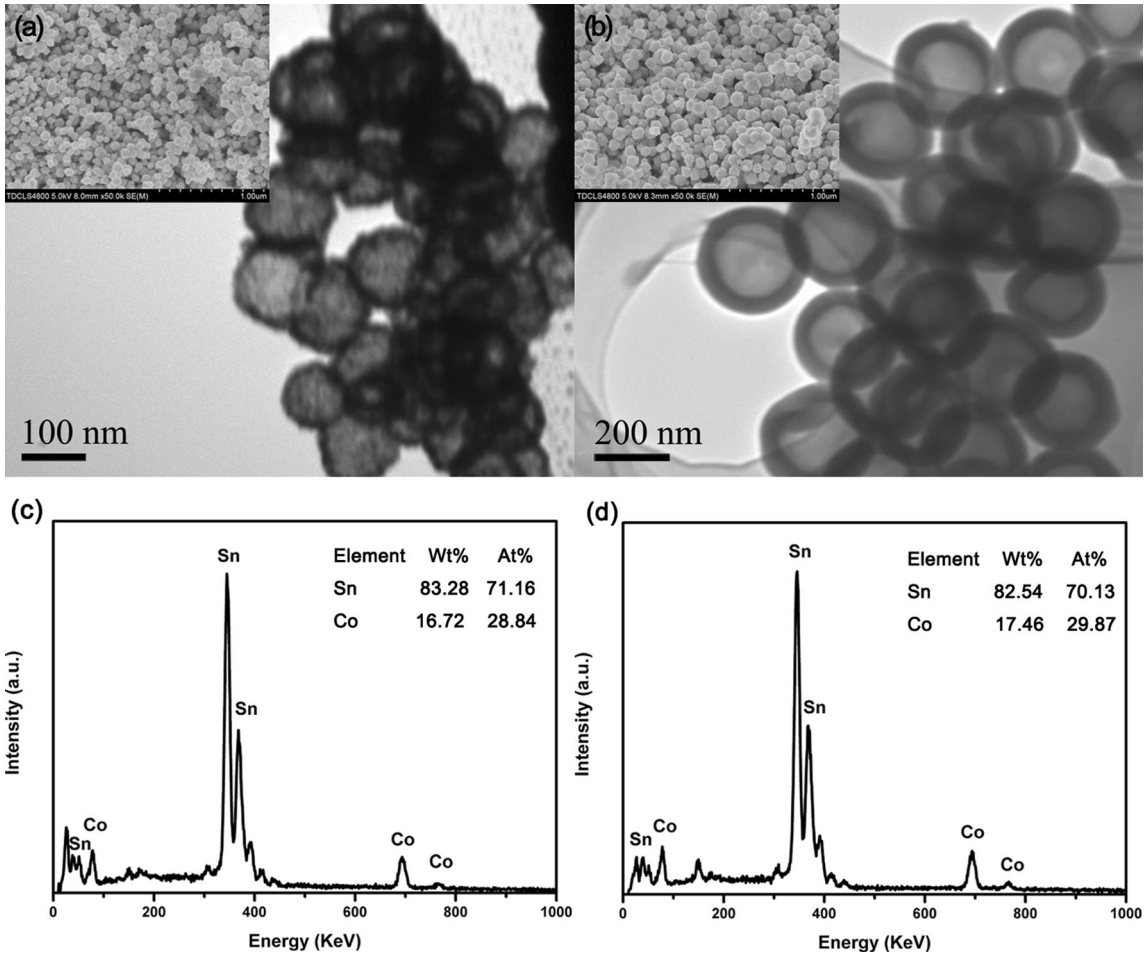

Fig. 2 TEM images of as-prepared hollow Sn-Co nanospheres: **a** sample 1 and **b** sample 2. The *insert images* are the corresponding SEM images of Co nanoparticles. The EDS spectrum with the corresponding element mass and atomic percentage of **c** sample 1 and **d** sample 2

galvanic replacement reaction will be initiated immediately. In the initial stage, the Co atoms from the surface of the solid nanoparticles can quickly react with Sn^{2+} ions to release Co^{2+} ions and electrons into the solution. Simultaneously, the Sn^{2+} ions are reduced into Sn atoms by capturing electrons and then deposited on the surface of the Co templates. With the reaction proceeding, the deposition will lead to a thin and incomplete shell of Sn on the surface of each nanoparticle. As shown in step 1, the void space between exterior shell and interior solid core is visible. This structural evolution can be confirmed by the TEM image at corresponding stage as shown in Fig. 4b. Accompanying the deposition of Sn, alloying will occur between Sn and Co atoms. Further prolonging the reaction time, the Co core becomes smaller, and consequently, the interior of nanoparticle gradually becomes empty, as shown in step 2. At the same time, the shell grows complete without small holes or opening, which can be attributed to the continuous deposition of Sn on the surface and a mass-transport process [37–39]. The TEM image in Fig. 4c verifies this speculation. In the later stage of reaction (step 3), a uniform hollow void with a pine-free shell has formed, which is in agreement with the TEM image in Fig. 4d.

The galvanostatic discharge-charge profiles of hollow Sn-Co-20 and Sn-Co-40 nanospheres are evaluated over a voltage range of 0.01 to 2.00 V at a current density of 100 mA g^{-1}, as shown in Fig. 5. In both cases, the voltage plateau at 0.3 V is observed, and the subsequent sloping regions gradually falling to 0.01 V are related to the lithiation of hollow Sn-Co nanospheres [40–44]. The irreversible capacity loss in the first cycle probably originates from the irreversible reduction of Sn-Co to Sn and the formation of solid electrolyte interface (SEI) film on the surface [42, 45].

In order to investigate the electrochemical behavior of electrodes, the first three CV curves of hollow Sn-Co-20 and Sn-Co-40 nanospheres are scanned at 0.1 mV s^{-1} and cycled between 0.001 and 2.0 V vs Li^+/Li, as shown in Fig. 6a, b, respectively. The CV curves of hollow Sn-Co-20 electrodes show the similar outline to that of hollow Sn-Co-40 electrodes, indicating that the electrochemical reaction mechanism of hollow Sn-Co electrodes is similar to each other. In both

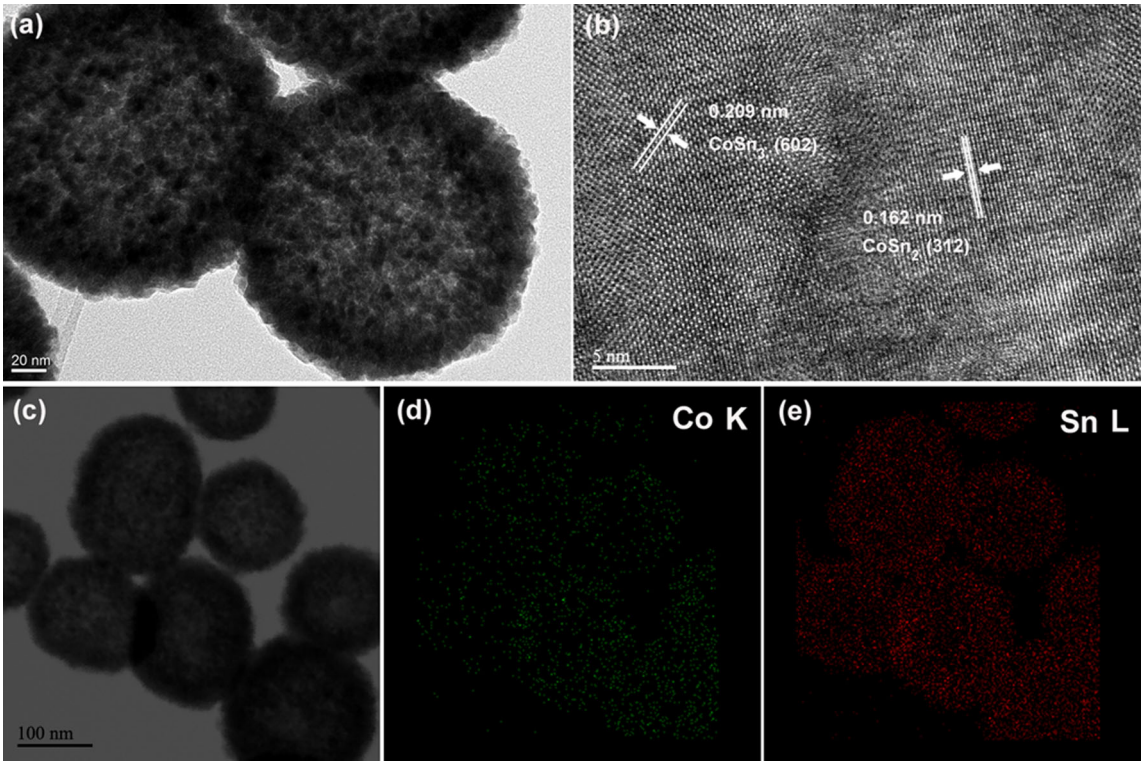

Fig. 3 **a**, **c** TEM image, **b** HRTEM image, and **d**, **e** images corresponding to Co and Sn mappings of hollow Sn-Co-20 nanospheres

cases, the reduction peaks at 0.25 V are due to the electrochemical reaction of Sn component in the Sn-Co alloy involving the formation of Li_xSn alloy [46, 47]. In contrast, the oxidation peaks are observed at 0.5 and 0.68 V, which is ascribed to a dealloying reaction from Li_xSn to form Li and Sn [41, 48]. These current-potential characteristics are in line with previous research studies on Sn-Co alloy anodes [49, 50]. Compared with hollow Sn-Co-40 nanospheres, the CV curves of hollow Sn-Co-20 nanospheres in the successive cycles are more overlapped, proving the better cycling stability of the electrodes consisting of hollow Sn-Co-20 nanospheres.

Figure 7 highlights the better cycling performance of the two types of hollow Sn-Co nanospheres than the pure ultra fine Sn nanoparticles at a current density of 100 mA g^{-1},

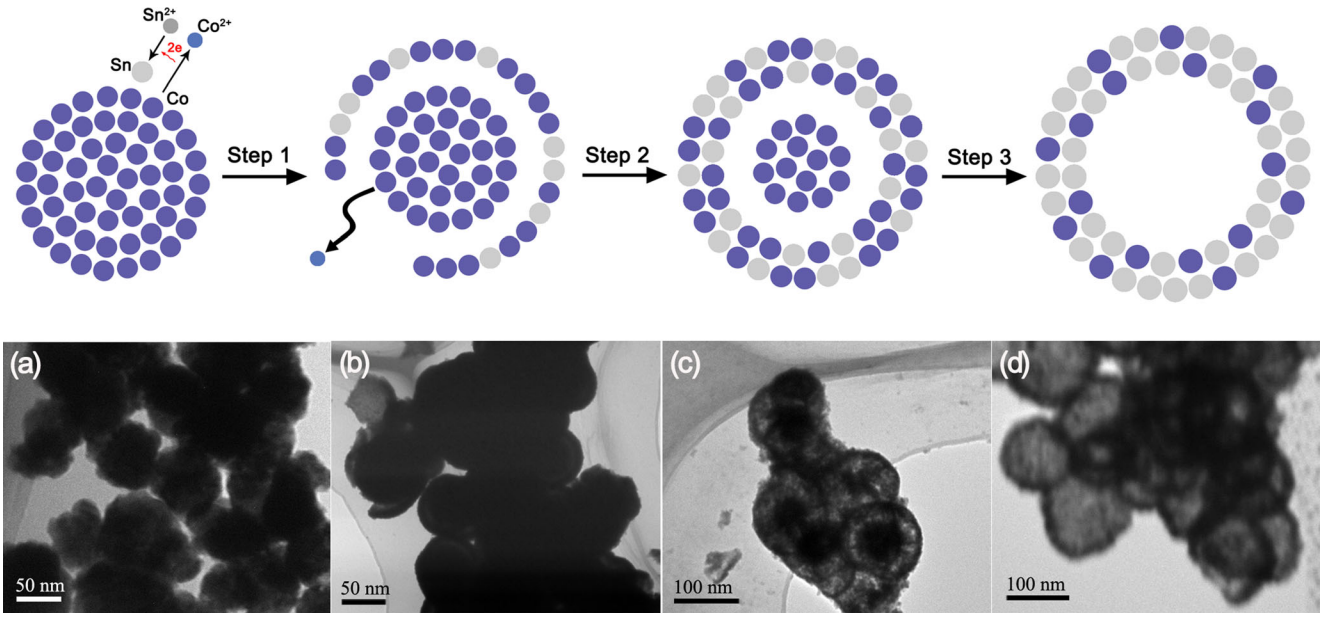

Fig. 4 Schematic illustration and the corresponding TEM images **a**–**d** of hollow Sn-Co nanospheres at different stages of galvanic replacement reaction

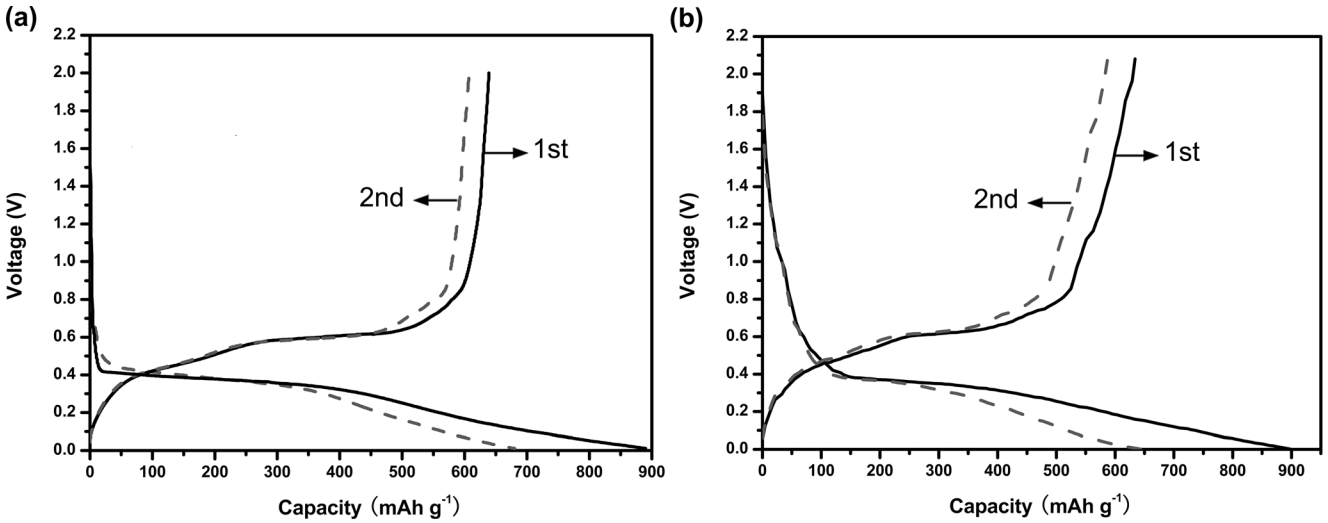

Fig. 5 Charge-discharge curves of **a** hollow Sn-Co-20 nanospheres and **b** hollow Sn-Co-40 nanospheres

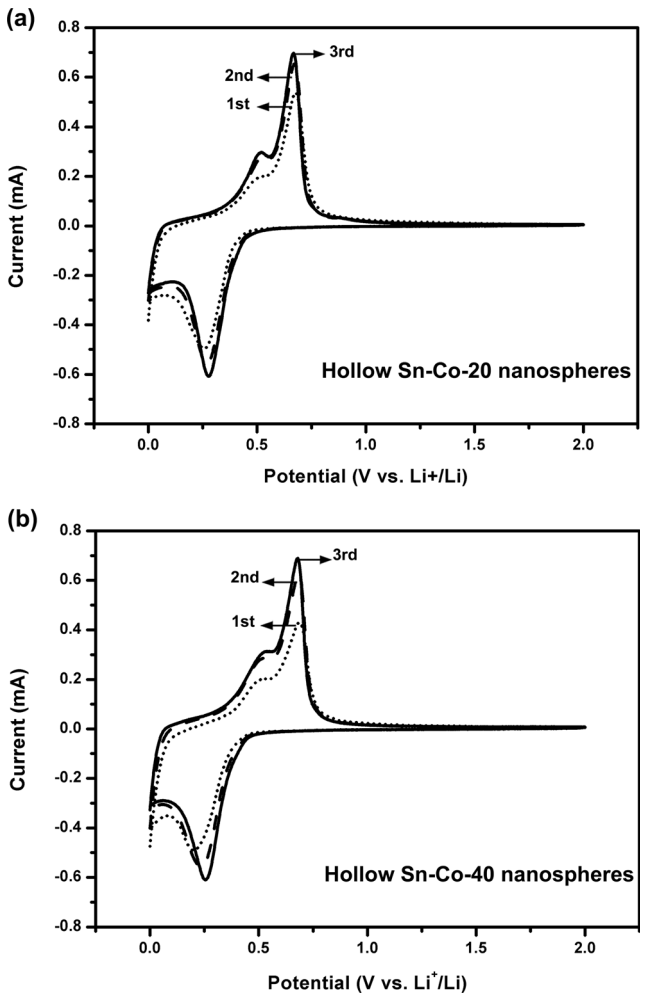

Fig. 6 Cyclic voltammetry of **a** hollow Sn-Co-20 nanospheres and **b** hollow Sn-Co-40 nanospheres for the first three cycles, at a scan rate of 0.1 mV s^{-1}

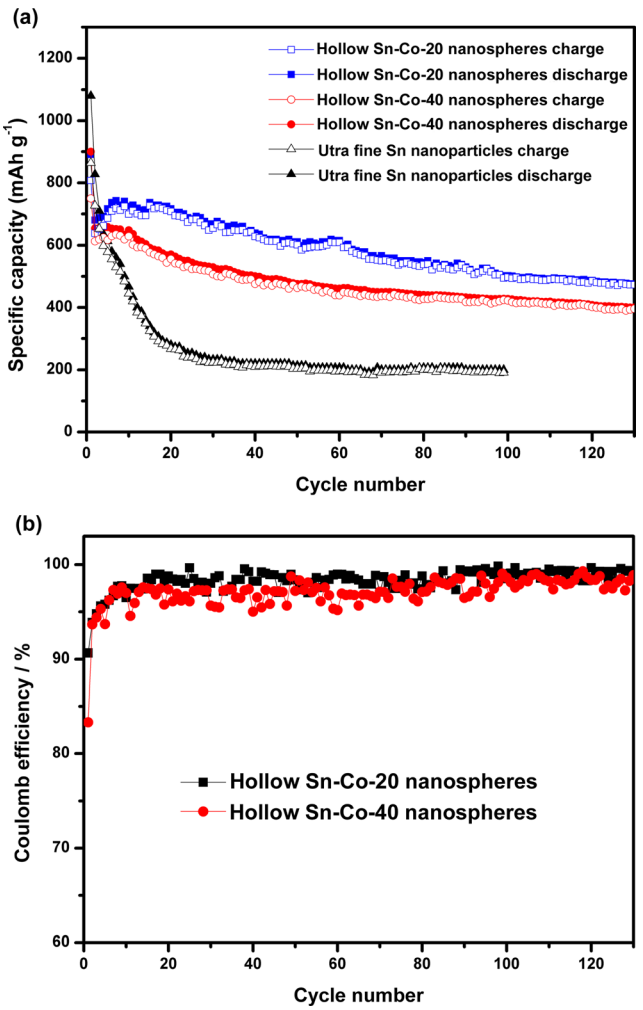

Fig. 7 **a** Cycling performance of hollow Sn-Co-20 nanospheres, hollow Sn-Co-40 nanospheres, and ultrafine pure Sn nanoparticles at a current density of 100 mA g^{-1}. **b** Coulomb efficiency of hollow Sn-Co-20 and hollow Sn-Co-40 nanospheres

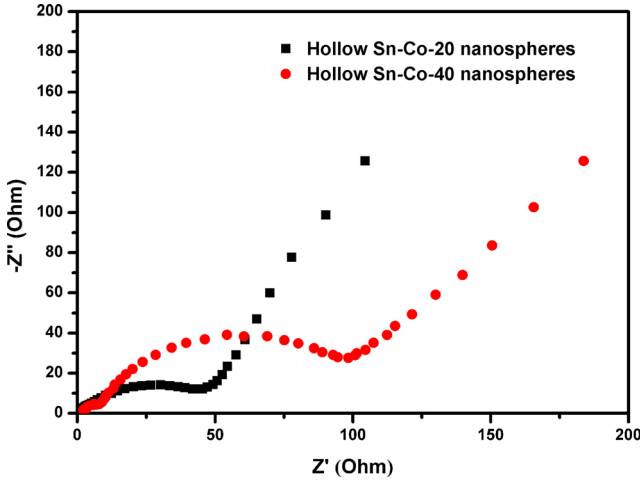

Fig. 8 Nyquist plots of hollow Sn-Co-20 and Sn-Co-40 nanospheres measured after fifth cycle

wherein hollow Sn-Co-20 nanospheres show the highest specific capacity. As shown in Fig. 7, the initial discharge capacity of ultra fine Sn nanoparticles is 1090 mAh g^{-1}, and the capacity decreases sharply in the following cycles and fades to only 200 mAh g^{-1} after 30th cycle. The abrupt degradation of capacity is the typical behavior for the pure Sn electrodes, which can be attributed to the electrical isolation of Sn from the current collector caused by the pulverization associated with extreme volume change in Sn during lithiation/delithiation [41, 51, 52]. By comparison with pure Sn, the hollow Sn-Co nanospheres show an enhanced electrochemical performance. For hollow Sn-Co-40 nanospheres, the initial discharge capacity is 900 mAh g^{-1}, and the reversible capacity drops to 613 mAh g^{-1} in the second cycle, with the first coulomb efficiency being 83.3 %. The capacity for the first ten cycles was even higher than 613 mAh g^{-1} and then gradually decreases. Finally, the hollow Sn-Co-40 nanospheres maintain a reversible capacity of 430 mAh g^{-1} after 100th cycle, with the coulomb efficiency being about 98 %. These results demonstrate that introduction of inactive Co element and hollow structure could partially alleviate the pulverization induced by the volume change of Sn [23, 24, 53, 54]. However, hollow Sn-Co-20 nanospheres with thin shell thickness show better cycling properties. The hollow Sn-Co-20 nanospheres exhibit a reversible capacity of 808 and 632 mAh g^{-1} in the first and second cycle, with the initial coulomb efficiency being 91.6 %. In addition, an increase in capacity in the subsequent several cycles can be observed. The hollow Sn-Co-20 nanospheres exhibit a steady reversible capacity of 502 mAh g^{-1} after 100th cycle, significantly higher than that of these counterparts. It is worth noting that the hollow Sn-Co-20 electrodes perform significantly better than recently reported tin-based electrodes [55–59] in terms of specific capacity and cycling stability. Abundant research has confirmed that the most stable electrochemical performance is found in $Sn_{1-x}Co_x$ alloy for $0.28<x<0.43$ [6, 50]. In the as-prepared hollow Sn-Co samples, $CoSn_2$

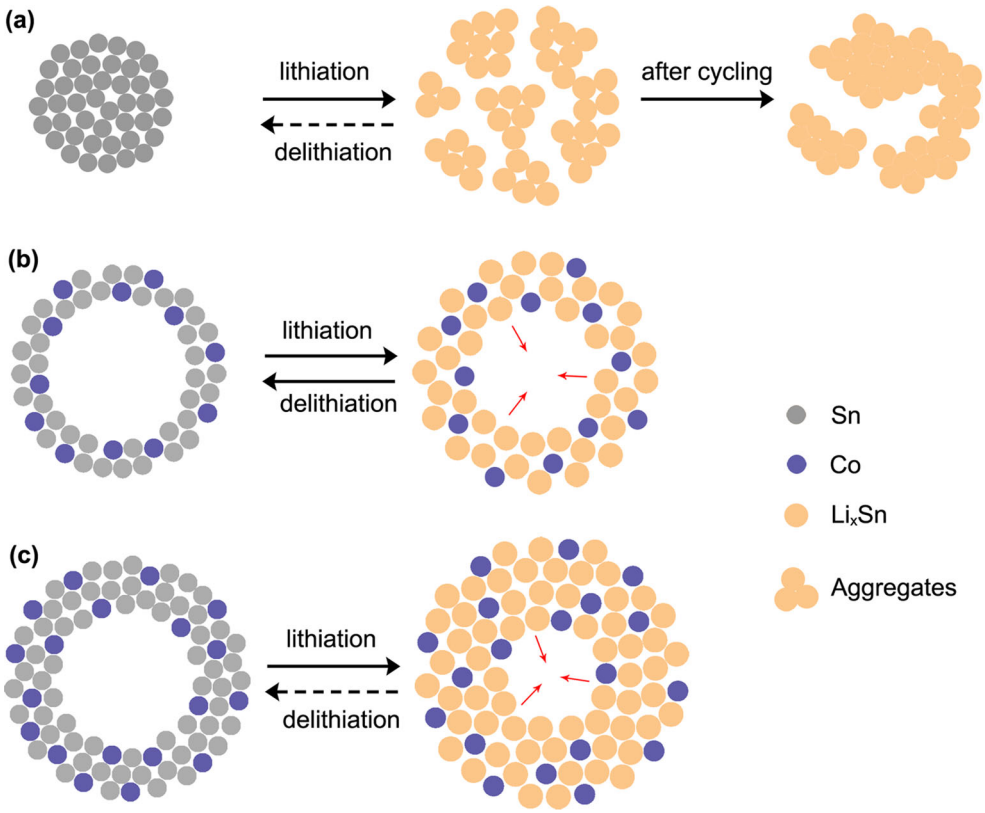

Fig. 9 The inference of electrochemical reaction of pure Sn nanoparticles and hollow Sn-Co nanospheres with different shell thickness on cycling performance

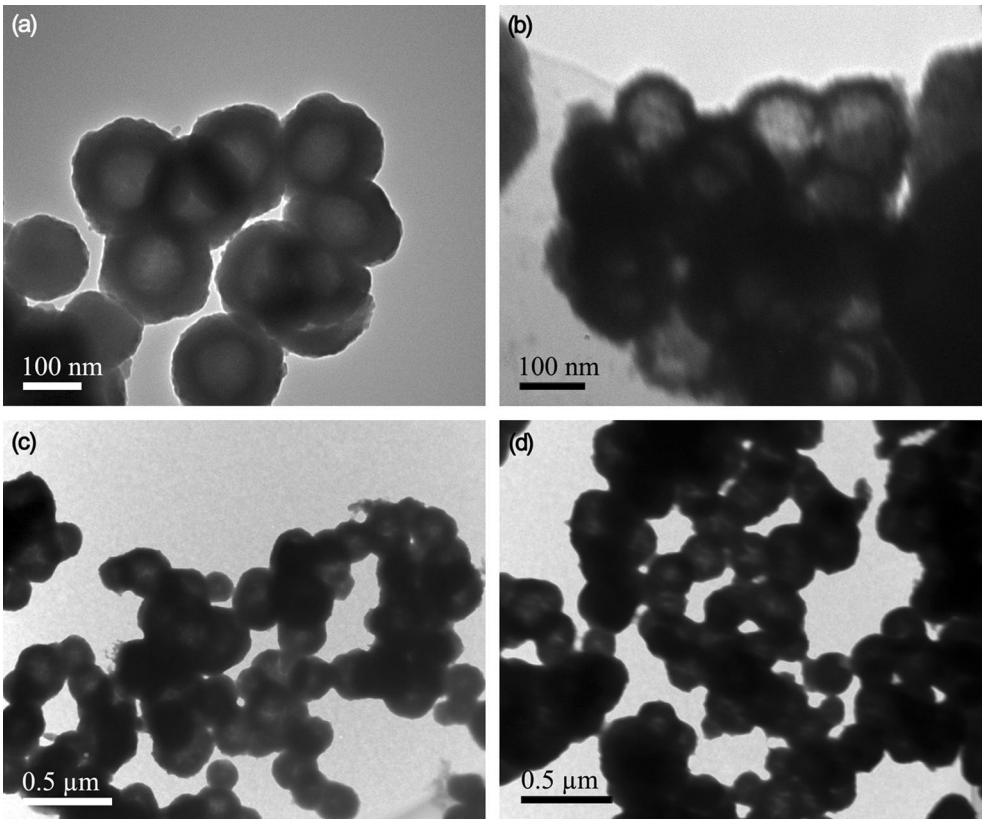

Fig. 10 TEM images of **a**, **b** hollow Sn-Co-20 nanospheres in lithiated and delithiated state, respectively, and **c**, **d** hollow Sn-Co-40 nanospheres in lithiated and delithiated state, respectively

phase plays a more important role in the improvement of electrochemical performance than $CoSn_3$ phase.

The electrochemical performance of hollow Sn-Co-20 nanospheres is superior to hollow Sn-Co-40 nanospheres, which can be attributed to the smaller size, thinner shell thickness and relatively large void volume of hollow Sn-Co-20 nanospheres. Firstly, the decrease in size and shell thickness provides short diffusion length and large contact area between liquid electrolyte and electrode, which are beneficial for the diffusion of the Li^+ during insertion/extraction process [23, 24]. Secondly, the hollow volume-occupying rate in hollow Sn-Co-20 nanospheres is about 48.6 %, whereas that of hollow Sn-Co-40 nanospheres is about 31.7 %. This suggests that hollow Sn-Co-20 nanospheres offer relatively large vacancy for the volume expansion and recovery in the lithiated/delithiated state, reinforcing the integrity of electrodes [21–24].

EIS measurement of the working electrodes is carried out to further investigate the contribution to superior electrochemical performance of hollow Sn-Co-20 nanospheres. As shown in Fig. 8, the Nyquist plots in both cases exhibit two distinct parts including a semicircle in the high and middle frequency region and a sloped line in the low frequency region. It is clear that the diameter of the depressed semicircle of hollow Sn-Co-20 nanospheres is much smaller than that of hollow Sn-Co-40 nanospheres, which reveals that hollow Sn-Co-20 nanospheres have lower contact and charge transfer resistance [60]. Moreover, hollow Sn-Co-20 nanospheres possess more

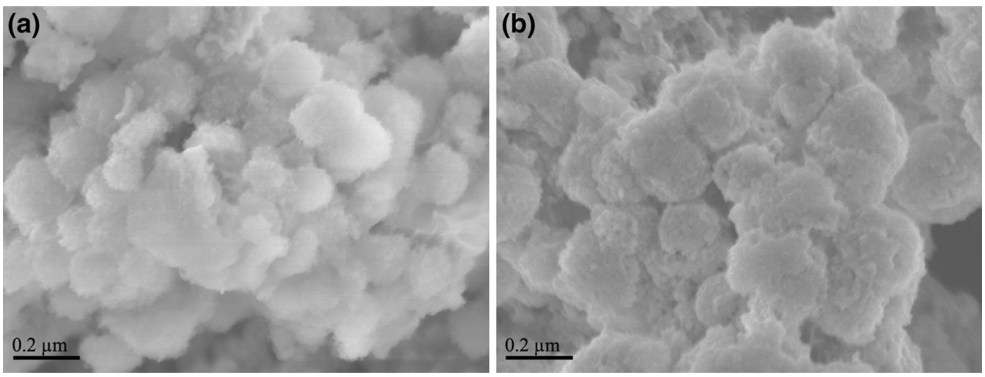

Fig. 11 SEM images of hollow Sn-Co nanospheres after cycling: **a** hollow Sn-Co-20 nanospheres and **b** hollow Sn-Co-40 nanospheres

straight inclined line in comparison to hollow Sn-Co-40 nanospheres, indicating that the Li^+ diffusion of hollow Sn-Co-20 nanospheres is faster [61]. These results imply that the combination of thin shell thickness and relatively large void space can facilitate the charge and Li^+ transfer.

Based on these experimental results, the discharge and charge mechanism for the solid Sn nanoparticles and hollow Sn-Co nanospheres with different shell thickness is displayed in Fig. 9. As observed in Fig. 9a, the large volume expansion from Sn to Li_xSn will result in the aggregation of Sn or Li_xSn particles, which will destroy spherical structure of the electrodes. In the case of hollow Sn-Co nanospheres configuration, small quality of inactive Co nanoparticles dispersed in Sn or Li_xSn can buffer the volume change and avoid the grain growth, shown in Fig. 9b, c. In addition, the hollow structure plays a more important role in accommodating the volume change. The interior void space allows the volume change to expand inward and outward rather than outward only.

The speculation above can be verified by the TEM images of hollow Sn-Co-20 and Sn-Co-40 nanospheres after cycling, as shown in Fig. 10. From Fig. 10a, c, similar structural evolution of hollow Sn-Co-20 and Sn-Co-40 nanospheres in the lithiated state can be observed. Due to the volume change of active materials, the shell becomes thicker and the void becomes smaller in the lithiated state. This is in agreement with the illustrations in Fig. 9b, c, further confirming that the hollow structure could accommodate the volume change. As displayed in Fig. 10b, the microstructure of hollow Sn-Co-20 nanospheres in the delithiated state shows less variation compared with the pristine samples, except for the slight increase in diameter. However, for hollow Sn-Co-40 nanospheres in the delithiated state, as shown in Fig. 10d, the void space is not as clear as the pristine samples. This suggests that the recovering process from the expanded state is not fully reversible for hollow Sn-Co-40 nanospheres. The discrepancy in both cases may be explained by the different volume-occupying rate in hollow Sn-Co-20 and Sn-Co-40 nanospheres. These results imply that a relatively large hollow volume-occupying rate in hollow configuration is favorable, especially for the anodes subjecting severe volume change.

The morphology of hollow Sn-Co-20 and Sn-Co-40 nanospheres after 100 cycles is shown in Fig. 11. For hollow Sn-Co-40 nanospheres, as shown in Fig. 11b, the slight aggregation and pulverization can be observed on the surface. This structural damage could lead to the decay of capacity upon cycling. Contrarily, the microstructure of hollow Sn-Co-20 nanospheres after 100 cycles is remained, due to the limited volume change. The well-defined morphology of hollow Sn-Co-20 nanospheres is consistent with their good electrochemical cycling performance.

Conclusion

Hollow Sn-Co nanospheres with different shell thickness and void size have been prepared by using Co nanoparticles as sacrificial templates via galvanic replacement reaction. Such a hollow structure offers sufficient void space, in which Sn-Co nanoparticles will experience a volume change without a collapse. In addition, the inactive Co element plays a role of matrix to accommodate the volume expansion and prevents the agglomeration of Sn nanoparticles. As anodes for LIBs, the hollow Sn-Co-20 nanospheres with thin shell exhibit a high capacity of 502 mAh g^{-1} after 100 cycles, which is superior to the corresponding counterparts. The enhancement is probably attributed to the small shell thickness and the relatively large void space of hollow Sn-Co-20 nanospheres as compared to hollow resultants with large shell thickness. Due to the facile synthesis and improved performance, it can be expected that the novel hollow Sn-Co alloy electrodes will pave the way for the development of the next generation of LIBs.

Acknowledgments This work was financially supported by the National Natural Science Foundation of China (No. 51143009 and 51273145).

References

1. Armand M, Tarascon JM (2008) Building better batteries. Nature 451:652–657
2. Tarascon JM, Armand M (2001) Issues and challenges facing rechargeable lithium batteries. Nature 414:359–367
3. Li H, Wang ZX, Chen LQ, Huang XJ (2009) Research in advanced materials for Li-ion batteries. Adv Mater 21:4593–4607
4. Rahul M, Rahul K, Toh-Ming L, Nikhil K (2012) Nanostructured electrodes for high-power lithium ion battery. Nano Energy 1:518–533
5. Beaulieu LY, Eberman KW, Turner RL, Krause LJ, Dahn JR (2001) Colossal reversible volume changes in lithium alloys. Electrochem Solid ST 4:A137–A140
6. Dahn JR, Mar RE, Abouzeid A (2006) Combinatorial study of $Sn_{1-x}Co_x$ ($0<x<0.6$) and $[Sn_{0.55}Co_{0.45}]_{1-y}C_y$ ($0<y<0.5$) alloy negative electrode materials for Li-ion batteries. J Electrochem Soc 153: A361–A365
7. Mackay DT, Janish MT, Sahaym U, Kotula PG, Jungjohann KL, Carter CB, Norton MG (2014) Template-free electrochemical synthesis of tin nanostructures. J Mater Sci 49:1476–1483
8. Zheng Y, Yang J, Nuli YN, Wang JL (2007) Nano-tin alloys dispersed in oxides for lithium storage materials. J Power Sources 174: 624–627
9. Hassoun J, Derrien G, Panero S, Scrosati B (2008) A nanostructured Sn-C composite lithium battery electrode with unique stability and high electrochemical performance. Adv Mater 20:3169–3175
10. Ferguson PP, Todd ADW, Dahn JR (2008) Comparison of mechanically alloyed and sputtered tin-cobalt-carbon as an anode material for lithium-ion batteries. Electrochem Commun 10:25–31
11. Wang F, Zhao MS, Song XP (2008) Nano-sized $SnSbCu_x$ alloy anodes prepared by co-precipitation for Li-ion batteries. J Power Sources 175:558–563

12. Todd ADW, Mar RE, Dahn JR (2007) Tin-transition metal-carbon systems for lithium-ion battery negative electrodes. J Electrochem Soc 154:A597–A604
13. Zhao HP, Jiang CY, He XM, Ren JG, Wan CR (2007) Advanced structures in electrodeposited tin base anodes for lithium ion batteries. Electrochim Acta 52:7820–7826
14. Simonin L, Lafont U, Kelder EM (2008) SnSb micron-sized particles for Li-ion batteries. J Power Sources 180:859–863
15. Wen ZG, Zheng F, Jiang ZR, Li MX, Luo YX (2013) Solvothermal synthesis of solid and hollow CoO nanospheres and their electrochemical properties in lithium-ion battery. J Mater Sci 48:342–347
16. Yu L, Wu HB, Lou XW (2012) Mesoporous $Li_4Ti_5O_{12}$ hollow spheres with enhanced lithium storage capability. Adv Mater 25: 2296–2300
17. Wang JY, Yang NL, Tang HJ, Dong ZH, Jin Q, Yang M, Kisailus D, Zhao HJ, Tang ZY, Wang D (2013) A accurate control of multishelled Co_3O_4 hollow microspheres as high-performance anode materials in lithium-ion batteries. Angew Chem Int Ed 52: 6417–6420
18. Wang B, Chen JS, Wu HB, Wang ZY, Lou XW (2011) Quasiemulsion-templated formation of alpha-Fe_2O_3 hollow spheres with enhanced lithium storage properties. J Am Chem Soc 133:17146–17148
19. Liu RQ, Li N, Xia GF, Li DY, Wang C, Xiao N, Tian D, Wu G (2013) Assembled hollow and core-shell SnO_2 microspheres as anode materials for Li-ion batteries. Mater Lett 93:243–246
20. Fang ZB, Huang JJ, He WJ, Zhang XS, Wu YP, Qing JW (2013) Electrochemical performance of SnO_2-Fe_2O_3 hollow spheres prepared by solid acid template method. Electrochim Acta 109:454–460
21. Lou XW, Archer LA, Yang ZC (2008) Hollow micro-/nanostructures: synthesis and applications. Adv Mater 20:3987–4019
22. Lai XY, Halperta JE, Wang D (2012) Recent advances in micro-/nano-structured hollow spheres for energy applications: from simple to complex systems. Energy Environ Sci 5:5604–5618
23. Liu J, Xue DF (2010) Hollow nanostructured anode materials for Li-ion batteries. Nanoscale Res Lett 5:1525–1534
24. Wang ZY, Zhou L, Lou XW (2012) Metal oxide hollow nanostructures for lithium-ion batteries. Adv Mater 24:1903–1911
25. Lou XW, Yuan CL, Archer LA (2007) Shell-by-shell synthesis of tin oxide hollow colloids with nanoarchitectured walls: cavity size tuning and functionalization. Small 3:261–265
26. Lou XW, Yuan CL, Archer LA (2007) Double-walled SnO_2 nanococoons with movable magnetic cores. Adv Mater 19:3328–3332
27. Hu J, Chen M, Fang XS, Wu LW (2011) Fabrication and application of inorganic hollow spheres. Chem Soc Rev 40:5472–5491
28. Fan HJ, Gosele U, Zacharias M (2007) Formation of nanotubes and hollow nanoparticles based on Kirkendall and diffusion processes: a review. Small 3:1660–1671
29. Yin YD, Rioux RM, Erdonmez CK, Hughes S, Somorjai GA, Alivisatos AP (2004) Formation of hollow nanocrystals through the nanoscale Kirkendall effect. Science 304:711–714
30. Cao HL, Qian XF, Wang C, Ma XD, Yin J, Zhu ZK (2005) High symmetric 18-facet polyhedron nanocrystals of Cu_7S_4 with a hollow nanocage. J Am Chem Soc 127:16024–16025
31. Sun YG, Xia YN (2002) Shape-controlled synthesis of gold and silver nanoparticles. Science 298:2176–2179
32. Xiong YJ, Wiley B, Chen JY, Li ZY, Yin YD, Xia YN (2005) Corrosion-based synthesis of single-crystal Pd nanoboxes and nanocages and their surface plasmon properties. Angew Chem Int Ed 44:7913–7917
33. Sun YG, Mayers BT, Xia YN (2002) Template-engaged replacement reaction: a one-step approach to the large-scale synthesis of metal nanostructures with hollow interiors. Nano Lett 2:481–485
34. Oh MH, Yu T, Yu SH, Lim B, Ko KT, Willinger MG, Seo DH, Kim BH, Cho MG, Park JH (2013) Galvanic replacement reactions in metal oxide nanocrystals. Science 340:964–968
35. Xia XH, Wang Y, Ruditskiy A, Xia YN (2013) 25th Anniversary article: galvanic replacement: a simple and versatile route to hollow nanostructures with tunable and well-controlled properties. Adv Mater 25:6313–6333
36. Fan X, Tang XN, Ma DQ, Bi P, Jiang AN, Zhu J, Xu XH (2014) Novel hollow Sn-Cu composite nanoparticles anodes for Li-ion batteries prepared by galvanic replacement reaction. J Solid State Electrochem 18:1137–1145
37. Batzill M, Koel BE (2004) Silver on Pt (100)-room temperature growth and high temperature alloying. Surf Sci 553:50–60
38. Sun YG, Xia YN (2004) Mechanistic study on the replacement reaction between silver nanostructures and chloroauric acid in aqueous medium. J Am Chem Soc 126:3892–3901
39. Zeng HC (2006) Synthesis architecture of interior space for inorganic nanostructures. J Mater Chem 16:649–662
40. Park CM, Kim JH, Kim H, Sohn HJ (2010) Li-alloy based anode materials for Li secondary batteries. Chem Soc Rev 39:3115–3141
41. Winter M, Besenhard JO (1999) Electrochemical lithiation of tin and tin-based intermetallics and composites. Electrochim Acta 45: 31–50
42. Tan CH, Qi GW, Li YP, Guo J, Wang X, Kong DL, Wang HJ, Zhang SY (2013) Performance enhancement of Sn-Co alloys for lithium-ion battery by electrochemical dissolution treatment. J Alloys Compd 574:206–211
43. Tamura N, Ohshita R, Fujimoto M, Kamino M, Fujitani S (2003) Advanced structures in electrodeposited tin base negative electrodes for lithium secondary batteries. J Electrochem Soc 150: A679–A683
44. Rhodes KJ, Meisner R, Kirkham M, Dudney N, Daniel C (2012) In Situ XRD of Thin Film Tin Electrodes for Lithium Ion Batteries. J Electrochem Soc 159:A294–A299
45. Chen ZX, Qian JF, Ai XP, Cao YL, Yang HX (2009) Preparation and electrochemical performance of Sn-Co-C composite as anode material for Li-ion batteries. J Power Sources 189:730–732
46. Amadei I, Panero S, Scrosati B, Cocco G, Schiffini L (2005) The Ni3Sn4 intermetallic as a novel electrode in lithium cells. J Power Sources 143:227–230
47. Zhang JJ, Xia YY (2006) Co-Sn alloys as negative electrode materials for rechargeable lithium batteries. J Electrochem Soc 153: A1466–A1471
48. Yang CG, Zhang DW, Zhao YB, Lu YH, Wang L, Goodenough JB (2011) Nickel foam supported Sn-Co alloy film as anode for lithium ion batteries. J Power Sources 196:10673–10678
49. Ui K, Kikuchi S, Jimba Y, Kumagai N (2011) Preparation of Co-Sn alloy film as negative electrode for lithium secondary batteries by pulse electrodeposition method. J Power Sources 196:3916–3920
50. Du Z, Zhang S (2011) Enhanced electrochemical performance of Sn-Co nanoarchitectured electrode for lithium ion batteries. J Phys Chem C 115:23603–23609
51. Idota Y, Kubota T, Matsufuji A, Maekawa Y, Miyasaka T (1997) Tin-based amorphous oxide: a high-capacity lithium-ion-storage material. Science 276:1395–1397
52. Beaulieu LY, Beattie SD, Hatchard TD, Dahn JR (2003) The electrochemical reaction of lithium with tin studied by in situ AFM. J Electrochem Soc 150:A419–A424
53. Xue LJ, Xu YF, Huang L, Ke FS, He Y, Wang YX, Wei GZ, Li JT, Sun SG (2011) Lithium storage performance and interfacial processes of three dimensional porous Sn-Co alloy electrodes for lithium-ion batteries. Electrochim Acta 56:5979–5987
54. Groult H, El Ghallali H, Barhoun A, Briot E, Julien CM, Lantelme F, Borensztjan S (2011) Study of Co-Sn and Ni-Sn alloys prepared

in molten chlorides and used as negative electrode in rechargeable lithium battery. Electrochim Acta 56:2656–2664
55. Yang R, Huang J, We Z, Lai WZ, Zhang XZ, Zheng J, Li XG (2010) Bubble assisted synthesis of Sn–Sb–Cu alloy hollow nanostructures and their improved lithium storage properties. J Power Sources 195:6811–6816
56. Fan XY, Ke FS, Wei GZ, Huang L, Sun SG (2009) Lithiation/delithiation performance of Sn–Co alloy anode using rough Cu foil as current collector. J Solid State Electrochem 13:1849–1858
57. Fan XY, Ke FS, Wei GZ, Huang L, Sun SG (2009) Sn-Co alloy anode using porous Cu as current collector for lithium ion battery. J Alloys Compd 476:70–73
58. He JC, Zhao HL, Wang MW, Jia XD (2010) Preparation and characterization of Co-Sn-C anodes for lithium-ion batteries. Mater Sci Eng B 171:35–39
59. Fan Q, Chupas PJ, Whittingham MS (2007) Characterization of amorphous and crystalline tin-cobalt anodes. Electrochem Solid ST 10:A274–A278
60. Choi N-S, Yan Y, Cui Y, Cho J (2011) One dimentioal Si/Sn based nanowires and nanotubes for lithium-ion energy storage materials. J Master Chem 21:9825–9840
61. Mahood N, Zhang C, Jiang J, Liu F, Hou Y (2013) Multifunctional CoS_4/Graphene composites for lithium ion battery and oxygen reduction reaction. Chem-Eur J 19:5183–51890